SANDIA REPORT
SAND200X-XXXX
Unlimited Release
Printed November 2016

A new approach to entangling neutral atoms

Jongmin Lee, Michael J. Martin, Yuan-Yu Jau, Ivan H. Deutsch and Grant W. Biedermann

Prepared by
Sandia National Laboratories
Albuquerque, New Mexico 87185 and Livermore, California 94550

Sandia National Laboratories is a multi-mission laboratory managed and operated by Sandia Corporation, a wholly owned subsidiary of Lockheed Martin Corporation, for the U.S. Department of Energy's National Nuclear Security Administration under contract DE-AC04-94AL85000.

Sandia National Laboratories

Issued by Sandia National Laboratories, operated for the United States Department of Energy by Sandia Corporation.

Available to DOE and DOE contractors from
U.S. Department of Energy
Office of Scientific and Technical Information
P.O. Box 62
Oak Ridge, TN 37831

Telephone: (865) 576-8401
Facsimile: (865) 576-5728
E-Mail: reports@osti.gov
Online ordering: http://www.osti.gov/scitech

Available to the public from
U.S. Department of Commerce
National Technical Information Service
5301 Shawnee Rd
Alexandria, VA 22312

Telephone: (800) 553-6847
Facsimile: (703) 605-6900
E-Mail: orders@ntis.gov
Online order: http://www.ntis.gov/search

SAND200X-XXXX
Unlimited Release
Printed November 2016

A new approach to entangling neutral atoms

Grant W. Biedermann, Jongmin Lee, Michael Martin, and Yuan-Yu Jau
Physics-Based Microsystems
Sandia National Laboratories
P.O. Box 5800
Albuquerque, New Mexico 87185-MS1082

Abstract

Our team has developed a new approach to entangling neutral atoms with a Rydberg-dressed interaction. Entangling neutral atoms is an essential key of quantum technologies such as quantum computation, many-body quantum simulation, and high-precision atomic sensors. The demonstrated Rydberg-dressed protocol involves adiabatically imposing a light shift on the ground state by coupling an excited Rydberg state with a tuned laser field. Using this technique, we have demonstrated a strong and tunable dipole-dipole interaction between two individually trapped atoms with energy shifts of order 1 MHz, which has been challenging to achieve in other protocols. During this program, we experimentally demonstrated Bell-state entanglement and the isomorphism to the Jaynes-Cumming model of a Rydberg-dressed two-atom system. Our theoretical calculations of a CPHASE quantum logic gate and arbitrary Dicke state quantum control in this system encourage further work.

ACKNOWLEDGMENTS

We thank A. Hankin for early contributions to the experiment, B. Keating for theoretical support and A. Orozco for latter contributions to the experiment.

CONTENTS

FIGURES

NOMENCLATURE

DOE	Department of Energy
SNL	Sandia National Laboratories
LDRD	Laboratory directed research and development
SWAP	Size, weight and power
GHZ	Greenberger–Horne–Zeilinger
EDDI	Electric dipole-dipole interaction
NMRF	Nano materials research foundation
UV	Ultra-violet
NA	Numerical Aperture
JC	Jaynes-Cummings
QED	Quantum electrodynamics
QUBO	Quadratic unconstrained binary optimization

INTRODUCTION

Entangling neutral atoms is the key component of quantum technologies such as quantum computation, many-body quantum simulation, and high-precision atomic sensors. Realization of quantum information processors is one of the ultimate goals of quantum technologies, which have been explored in several platforms ranging from trapped ions and neutral atoms to superconducting microwave circuits. Controlled entanglement of neutral atoms has been challenging, particularly if one seeks tunable interactions that are strong, coherent and long-range. The Rydberg blockade achieves strong, long-range coupling. This has been successfully employed for implementing controlled entangling interactions between atoms and quantum logic gates. In the standard protocol, short pulses excite the population of one atom to the Rydberg state and optical excitation of a second atom is blockaded because of the electric dipole-dipole interaction (EDDI).

In this LDRD, we explored a new approach to entanglement, a Rydberg-dressed interaction, which uses Rydberg-dressed atoms, an admixture of a ground state atom (long coherence time) and a Rydberg state atom (strong dipole-dipole interaction). The Rydberg-dressed entanglement protocols can be extended to many atoms in principle. This Rydberg-dressed interaction enables tunable, anisotropic interactions that open the door to quantum simulations of a variety of exotic quantum phases. In addition, it allows for quantum control of interacting atoms based solely on microwave/radiofrequency fields whose phase coherence is easily maintained. The created many-atom entangled state can be exploited as an input state to quantum sensors for high precision metrology.

Quantum sensors such as atom interferometers, atomic magnetometers, and atomic clocks may be one of the more near-term quantum technologies. The sensitivity of quantum sensors can be significantly improved by many-atom entanglement such as spin-squeezing, or full entanglement such as the GHZ state. For example, a fully entangled system of 100 atoms can perform a precision measurement 100 times faster than a non-entangled sample of the same number. Considering that most non-entangled atom interferometers with $\gg 10^4$ atoms, operate with a signal-to-noise ratio similar to that of 100 entangled atoms, it is clear that system SWAP requirements could be significantly reduced by operating with a small, entangled sample.

Beyond quantum sensing, this achievement has important ramifications for quantum computation and simulation. For example, a scalable digital quantum computation can be pursued based on universal phase gates. Furthermore, the tunable nature of the interaction lends itself well to adiabatic quantum computation and simulation. The study of quantum simulation will help to design new functional materials or develop new devices. Quantum simulation of complex materials is essential for understanding physical phenomena such as quantum frustration, magnetic/topological order, equilibration, spin liquids, transport, strong correlations, localization, phase transitions, and high Tc superconductivity. This owes to the fact that modeling of complex materials requires excessive numerical computing resources. Exact numerical solutions require exponentially scaling classical resources compared to polynomial-scaling quantum resources as the problem size grows.

Project vision

Quantum information processing is a powerful approach to manipulating information for computing, simulation and sensing. Developing the building blocks for this technology has been challenging and has been pursued on a variety of platforms. Due to the unique possibilities for sensing and simulation, neutral atoms are an attractive platform. However, realizing a strong and tunable entangling interaction has been difficult. In this project, we proposed to demonstrate a new Rydberg-Dressed approach to coherent interactions of neutral atoms. The Rydberg-Dressed approach affords a tunable interaction, unique opportunities for quantum control, and different environmental sensitives that can lead to a better entanglement fidelity. We built the experimental work upon the previously developed apparatus of the AQUARIUS grand challenge LDRD. We engaged Prof. Ivan H. Deutsch at the University of New Mexico to provide theoretical guidance.

Project structure, and participants

Structure

We structured the project as an exploratory demonstration effort supported by theoretical expertise. The theoretical support was led by Prof. I. H. Deutsch at the University of New Mexico. The overall project and experimental effort was led by Grant Biedermann.

Participants

The project clearly benefited from a complimentary team of experts from the experimental atomic physics, and quantum information science communities. The technical participants included:

Team member	**Role**
Grant Biedermann	Project lead
Prof. Ivan Deutsch	Theory lead
Aaron Hankin	PhD student: experiment
Yuan-Yu Jau	Staff: Theory and Experiment
Jongmin Lee	Postdoc: experiment
Michael Martin	Truman Postdoc: experiment
Bob Keating	PhD student: theory
Elizabeth Kim	Naval Academy undergraduate: experiment
Adrian Orozco	PhD student: experiment
Rob Cook	Postdoc: Theory

SUMMARY OF ACCOMPLISHMENTS

Overview

The project was a three-year NMRF LDRD project that began in October 2013 and concluded in September 2016. The total funding of the project was $1.645 M. We developed a coherent Rydberg spectroscopy system using direct excitation with a single UV photon that is limited only by the fundamental Rydberg state lifetime. We demonstrated for the first time, a Rydberg-dressed interaction between two atoms and measured the dependence upon interatomic distance using adjustable optical tweezers. We invented and demonstrated a spin-flip blockade entangling technique using a Rydberg-dressed interaction that resulted in a new record entanglement fidelity. We invented and demonstrated a controlled-phase entangling gate technique using adiabatic dressing that is extendable to multiple atoms. We developed key techniques for quantum simulation using a Rydberg-Dressed interaction that allow simulation beyond the Ising model.

Single-photon Rydberg spectroscopy

We have demonstrated a single-photon UV laser system for Rydberg-state excitation [1], and this scheme offers the advantages of a longer coherence time, and the simple and reliable coherent manipulation of a Rydberg transition compared to the two-photon excitation scheme. In addition, we implemented electric field controllability [2] with electrodes and a grounded electric-field shielding structure that minimizes stray electric fields and stabilizes electric field drifts improving the Rydberg spectroscopy.

Single-photon Rydberg UV laser system

A single-photon Rydberg state excitation and Rydberg blockade has been demonstrated with a 319nm UV laser system. We measure and control the electric field environment to enable coherent control of Rydberg states. With this coherent control, we demonstrate Rydberg blockade of two atoms. Compared to two-photon excitation methods, this single-photon approach significantly reduces channels for decoherence through photon scattering and ac Stark shifts from the intermediate state. The moderate increase in Doppler sensitivity when using single-photon Rydberg excitation can be addressed with more advanced cooling techniques, such as ground-state cooling as well as multi-photon approaches.

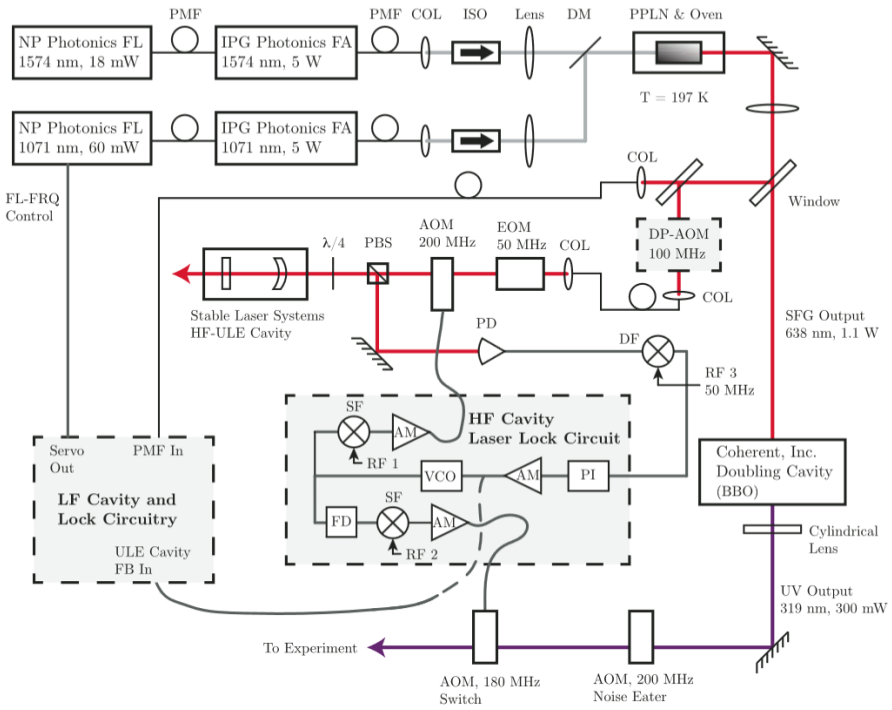

Figure 1: Diagram of a single-photon Rydberg excitation UV laser system [1]. $\boldsymbol{\lambda/4}$: quarter-wave plate; AM: voltage amplifier; COL: fiber collimation package; FA: fiber amplifier; FB: feedback; FD: frequency doubling; FL: fiber laser; FL-FRQ: voltage control of fiber laser frequency; ISO: optical isolator; LF: low finesse; PD: photodiode; PI: proportional-integral feedback; PMP: polarization maintaining fiber; SF: sum frequency; rf: radio frequency source; VCO: voltage controlled oscillator.

Figure 1 shows that frequency summing in a PPLN crystal of two fiber laser system yields 638-nm light and frequency doubling of this light in a BBO generates UV light at 319 nm. The 638-nm laser frequency is stabilized using a multi-staged servo with an ultralow expansion (ULE), high-finesse (HF) cavity as the primary reference.

Electric field control with electrodes

We nullify stray electric fields near the Rydberg atoms by applying voltages to eight electrodes surrounding the optical tweezers. The grounded electric-field shielding structure surrounds all environments except a high NA lens and an optical window along the direction of the optical tweezer. Since the electric field control system reduces the dc Stark shift of the 319-nm Rydberg transition and leads to a narrower 319-nm transition linewidth, this system enhances the spectroscopic demonstration of Rydberg states.

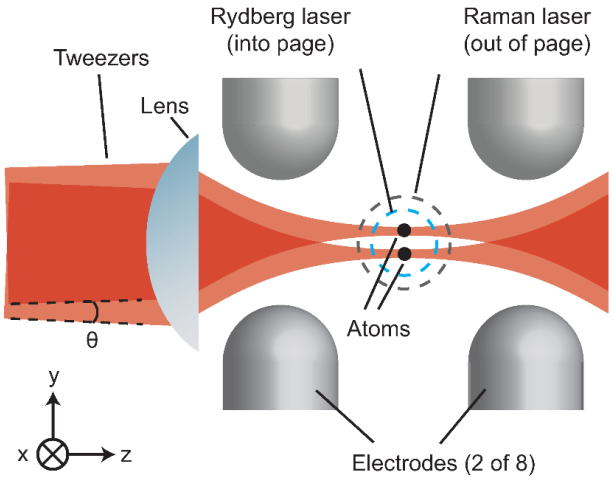

Figure 2. Electric field control system with electrodes [2].

Figure 2 shows the electric field control system with eight electrodes. The grounded electric-field shielding structure (not shown) surrounds them. The Rydberg laser and the Raman lasers are aligned along the x-axis. Two optical tweezers are formed by two lasers with an angular separation θ. In this set-up, eight electrodes nullify stray electric fields around the trapped atoms. The bias magnetic field for a quantization axis is applied along the x-axis.

The large polarizability of a high principal quantum number n Rydberg state gives rise to exotic many-body interactions as well as an extreme sensitivity to the electric field environment. Precision spectroscopy of such states allows for a variety of exciting demonstrations in metrology, fundamental quantum mechanics, and quantum information. For example, cold Rydberg atoms employed as near-surface electric field sensors could characterize both field amplitude and source. This includes experiments that explore near-surface field spectral density, induced dipole moments for surface adatoms, and insulator charging on an atom chip. Large Rydberg state polarizabilities also enable long-range electric dipole-dipole interactions (EDDIs) between Rydberg atoms, yielding strongly correlated systems through the Rydberg blockade effect. Recent experiments use Rydberg blockade to observe entanglement between neutral atoms, a controlled-NOT quantum gate, and collective many-body Rabi oscillations.

Rydberg-dressed interaction

Cold neutral atoms are attractive as the ability to create entanglement between atoms would allow for greatly increased precision of interferometers for applications in clocks, field sensors, and force sensors. In addition, cold atoms provide a natural platform for quantum simulation of condensed-matter physics and scalable digital quantum computers. Controlled entanglement of neutral atoms has been challenging, particularly if one seeks tunable interactions that are strong, coherent and long-range.

The Rydberg blockade with a strong and long-range coupling has been successfully employed for implementing controlled entangling interactions between atoms and quantum logic gates. In this protocol, short pulses excite the population of one atom to the Rydberg state and optical excitation of a second atom is blockaded because of the electric dipole-dipole interaction (EDDI).

An alternative protocol is to adiabatically dress the ground state with the excited Rydberg state. This Rydberg-dressed interaction enables tunable, anisotropic interactions that open the door to quantum simulations of a variety of exotic quantum phases. In addition, it allows for quantum control of interacting atoms based solely on microwave/radio frequency fields whose phase coherence is easily maintained. Applications include spin-squeezing for metrology and quantum computing.

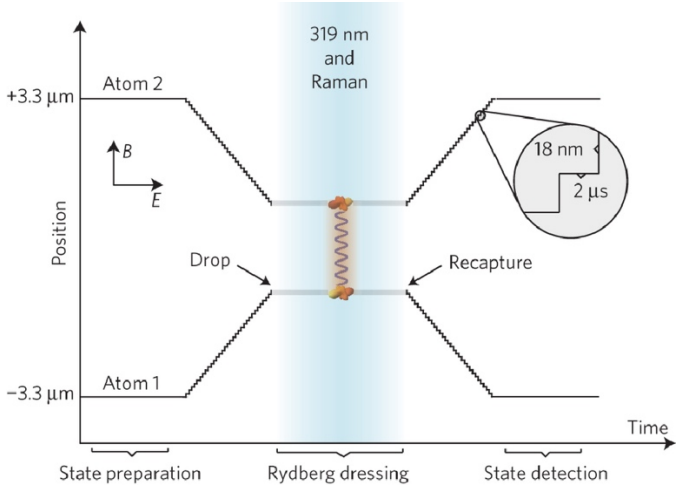

Figure 3. Experimental sequence of Rydberg-dressed interaction [3].

To achieve both a strong ground-state atom–atom interaction and a high-fidelity signal detection, the following experimental sequence has been used as shown in Fig. 3. The two state-prepared atoms held by optical tweezers translate towards each other. At a target distance, the Rydberg-dressing laser turns on to illuminate the two atoms simultaneously with a Raman laser and no optical tweezers. The two recaptured atoms translate back to the original positions for state detection.

Here we present a clear measurement of this interaction between two Rydberg-dressed atoms and employ coherent control in the ground-state manifold to demonstrate a full Rydberg-dressed spectrum analogous to the Jaynes-Cummings model, and also create entangled Bell states.

Jaynes-Cumming ladder of Rydberg-dressed atoms

We observe the nonlinearity of the Jaynes-Cummings (JC) ladder in the Autler-Townes spectroscopy of the hyperfine ground states for a Rydberg-dressed two-atom system. Here we summarize our results in [2]. Here the role of the two-level system in the JC model is played by the presence of a collective Rydberg excitation, and the bosonic mode manifests as the number n of single atom spin flips, symmetrically distributed between the atoms. We measure the normal-mode splitting and $\sqrt{n}$ nonlinearity as a function of detuning and Rabi frequency, thereby experimentally establishing the isomorphism with the JC model.

The Jaynes-Cummings (JC) model describes the interaction between a two-level atom and a single mode of the quantized electromagnetic field. Originally introduced in the context of cavity quantum electrodynamics (QED) for single atoms. More generally, the JC model describes a spin-boson system where a qubit is coupled to a bosonic mode. At its base is the spectrum of dressed states, the well-known JC ladder, which exhibits nonlinear normal-mode splitting proportional to $\sqrt{n}$, for n bosons coupled to the qubit on resonance. This nonlinearity is responsible for the collapse and revival of Rabi oscillations, and the generation of non-classical states, such as squeezed states and cat states.

Here we perform spectroscopy on a completely different instantiation of the JC model: symmetric Rydberg-blockaded atomic ensembles. In this system, the dressed states of the JC ladder are the laser-induced Rydberg-dressed states. The normal mode splitting is intimately related to the Autler-Townes splitting of the light shifted states.

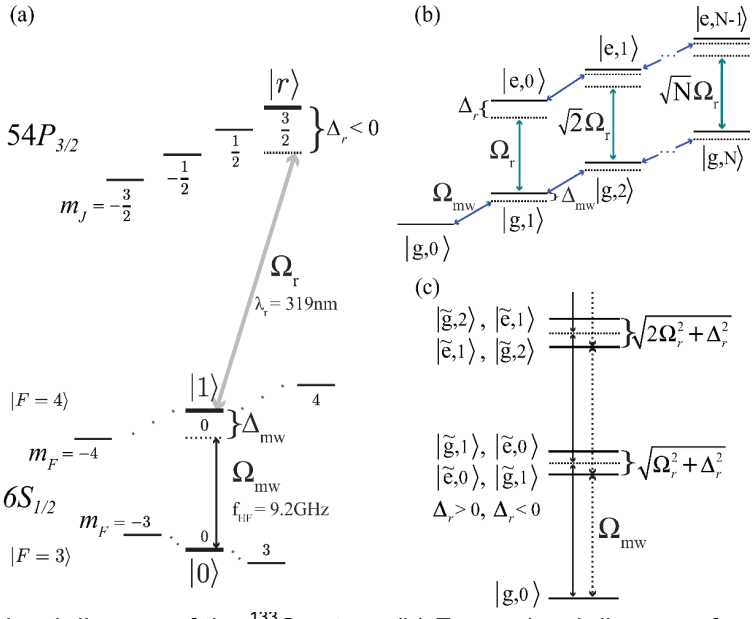

Figure 4. (a) Energy level diagram of the ^{133}Cs atom. (b) Energy level diagram of an ensemble of N bare state atoms, symmetrically coupled under the assumption of a perfect Rydberg blockade. (c) Energy level diagram of dressed ground state atoms showing the Autler-Townes splitting and exhibiting the nonlinearity of the JC model [2], where the states are $|0\rangle = |6S_{1/2}, F = 3, m_F = 0\rangle$ and $|1\rangle = |6S_{1/2}, F = 4, m_F = 0\rangle$, where Δ_r is the detuning from $|1\rangle$ to $|r\rangle = |54P_{3/2}, m_J = +3/2\rangle$ transition.

Figure 4 (a) shows an energy level diagram of the ^{133}Cs atom, and figure 4 (b) shows an energy level diagram of an ensemble of N bare state atoms, symmetrically coupled under the assumption of a perfect Rydberg blockade; $|g,n\rangle \equiv \{|0\rangle^{\otimes N-n}|1\rangle^{\otimes n}\}_{sym}$ and $|e,n\rangle \equiv \{|0\rangle^{\otimes N-n-1}|1\rangle^{\otimes n}|r\rangle\}_{sym}$. Figure 4 (c) shows an energy level diagram of dressed ground state atoms showing the Autler-Townes splitting and exhibiting the nonlinearity of the JC model. The states of $|\tilde{g},n\rangle$ and $|\tilde{e},n-1\rangle$ are the ground-like and Rydberg-like dressed states, respectively; $|\tilde{g},n\rangle \equiv \cos(\theta_n/2)\,|g,n\rangle + \sin(\theta_n/2)|e,n-1\rangle$ and $|\tilde{e},n-1\rangle \equiv \cos(\theta_n/2)|e,n-1\rangle - \sin(\theta_n/2)|g,n\rangle$, where $tan\theta_n = \sqrt{n}\Omega_r/\Delta_r$.

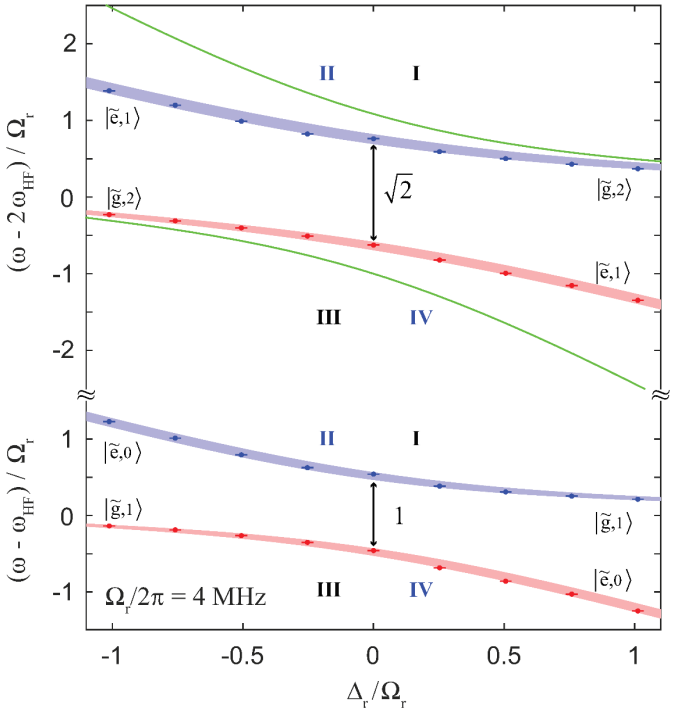

Figure 5. Jaynes-Cummings ladder and its nonlinearity for two Rydberg-dressed atoms [2].

In figure 5, Jaynes-Cummings ladder and its $\sqrt{n}$ nonlinearity for two Rydberg-dressed atoms are demonstrated. The x-axis is the normalized Rydberg detuning, and the y-axis is the normalized microwave detuning. For two-atom Rydberg-dressed states, the ground-like dressed states of $|\tilde{g},2\rangle$ are located the upper quadrant I and III, and the Rydberg-like dressed states of $|\tilde{e},1\rangle$ are located the upper quadrant II and IV. For single-atom Rydberg-dressed states, single-atom Rydberg dressed states of $|\tilde{g},1\rangle$ are positioned at the lower quadrant I and III, and single-atom Rydberg dressed states of $|\tilde{e},0\rangle$ are positioned at the lower quadrant II and IV. The upper/lower quadrant I and III (II and IV) are related to the ground-like (Rydberg-like) dressed states. The red (blue) bands are theoretical predictions of the microwave frequencies for the Autler-Townes splitting, incorporating measured systematic drifts (5%) in the experimental parameters (Δ_r and Ω_r). The green lines correspond to the energy of two atoms without the interaction. Two Rydberg transitions are considered for the theoretical plots, and $|6S_{1/2},F=4,m_F=0\rangle \rightarrow |54P_{3/2},m_J=+3/2\rangle$ and $|54P_{3/2},m_J=+1/2\rangle$. The Rabi frequencies of $m_J=+3/2$ and $+1/2$ are Ω_r and

$\Omega_r/\sqrt{3}$, respectively. States with $m_J = +3/2$ and $+1/2$ are separated by $\Delta_{Zeeman} \simeq 2.13\Omega_r$ with a 4.6 G magnetic field.

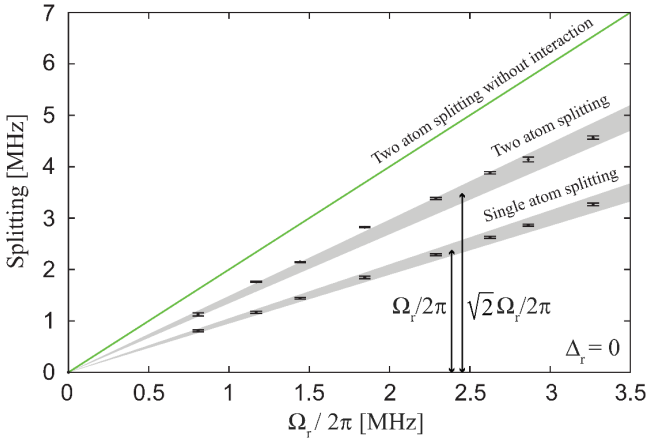

Figure 6. Resonant Autler-Townes splitting of two Rydberg-dressed atoms as a function of Rydberg-transition Rabi frequency [2], where $\Delta_r \approx 0$.

In figure 6, resonant ($\Delta_r \approx 0$) Autler-Townes splitting of two Rydberg-dressed atoms as a function of Rydberg-transition Rabi frequency is measured. The x-axis is the Rabi-frequency of a single-atom Rydberg excitation (Ω_r), and the y-axis is the Autler-Townes splitting measured by microwave spectroscopy. The two upper and lower data trends are the splittings of two-atom Rydberg-dressed states between $|\tilde{g}, 2\rangle$ and $|\tilde{e}, 1\rangle$ and single-atom Rydberg-dressed states between $|\tilde{g}, 1\rangle$ and $|\tilde{e}, 0\rangle$. The two gray bands incorporate measured systematic drifts (5%) in the experimental parameters (Ω_r and Δ_r). The green line corresponds to the splitting of two atoms without the interaction. Based on linear fits, the ratio of the splittings is $1.43(0.03)$, consistent with $\sqrt{2}$.

We directly observe the full spectrum of the JC ladder and its $\sqrt{n}$ nonlinearity in a two-atom Rydberg-dressed system. The normal-mode splitting of symmetric atomic ensembles with a Rydberg-blockade is the hallmark of the nonlinear coupling of the JC model. Furthermore, the full spectrum of the Rydberg-dressed states could offer a new approach to creating entanglement, operating phase gates, and generating arbitrary quantum states. Such a system can be also exploited for quantum control or a collective quantum logic gate using Rydberg super atoms. For example, with highly efficient single-atom loading and a $\sim$10μm Blockade radius, this could be extended to an ensemble of $\sim$100 atoms in 3D lattices.

Spin-flip blockade using the Rydberg-dressed interaction

The spin degrees of freedom of hyperfine ground state atoms provide a good platform for quantum information due to the long coherence time and controllability. However, the creation of strong coherent coupling between spins has been challenging. Here we summarize our work in [3] where we demonstrated a strong and tunable Rydberg-dressed interaction between two individually trapped neutral atoms with an energy shift of order 1MHz. This strong interaction leads to a ground-state spin-flip blockade, whereby simultaneous hyperfine spin flips of two atoms are inhibited owing to their mutual interaction. We employ this spin-flip blockade to rapidly produce single-step Bell-state entanglement between two atoms with a fidelity ~81(2)%.

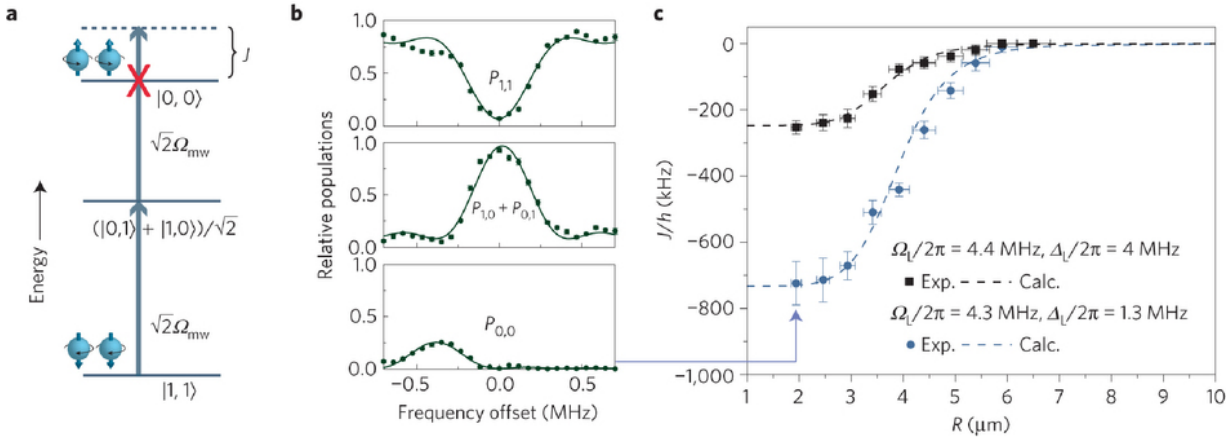

Figure 7. Rydberg-dressed ground-state interaction J and the spin-flip blockade [3], where $|0\rangle = |6S_{1/2}, F = 4, m_F = 0\rangle$, $|1\rangle = |6S_{1/2}, F = 3, m_F = 0\rangle$, and $|r\rangle = |64P_{3/2}, m_J\rangle$.

Figure 7 demonstrates a Rydberg-dressed ground-state interaction J and the spin-flip blockade. Figure 7 (a) shows an energy-level diagram of the spin-flip blockade on the Rydberg-dressed two-qubit sublevels. For a sufficiently large J, only the transition from $|1,1\rangle \rightarrow (|1,0\rangle$ or $|0,1\rangle)$ is allowed and the double spin-flip transition from $(|1,0\rangle$ or $|0,1\rangle) \rightarrow |0,0\rangle$ is blockaded when microwave radiation (stimulated Raman transition) is applied at the non-interacting, single-atom qubit resonance frequency. Figure 7 (b) shows a scan of the microwave frequency of the stimulated Raman pulse applied to the two Rydberg-dressed ^{133}Cs atoms. This reveals the ground-state spin-flip blockade. The excitation from $|1,1\rangle \rightarrow |0,0\rangle$ occurs through an anti-blockade two-photon transition. J/h is twice the shift of the resonance frequency for excitation to the state $|0,0\rangle$. Figure 7 (c) shows experimental data of J versus R with two sets of parameters. The dashed curves are the calculated values based on a detailed model with no free parameters.

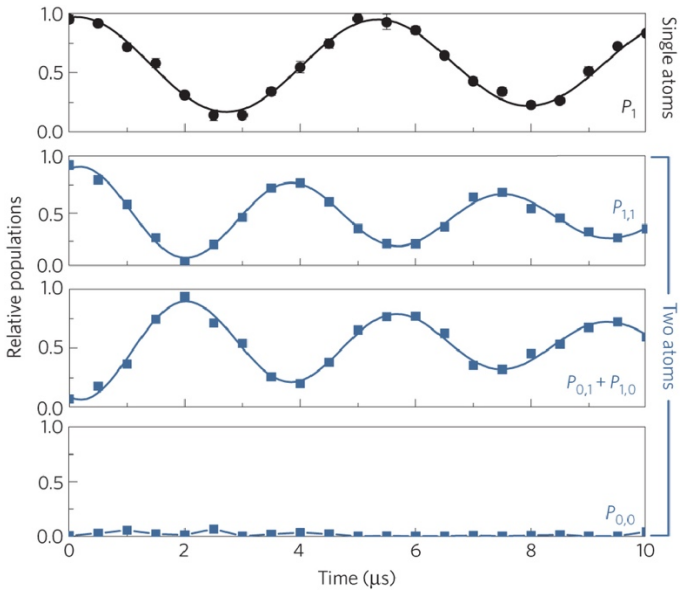

Figure 8. Generating entanglement directly [33], where $|0\rangle = |6S_{1/2}, F = 4, m_F = 0\rangle$, $|1\rangle = |6S_{1/2}, F = 3, m_F = 0\rangle$, and $|r\rangle = |64P_{3/2}, m_J\rangle$.

Figure 8 shows the generation of entanglement directly with a two-atom Rydberg-dressed spin-flip blockade interaction. The top panel shows Rabi oscillations of a single Rydberg-dressed Cs qubit. The lower three panels show two-atom data with Rydberg-dressed spin-flip blockade ($J \approx h \cdot 750\text{kHz}$ with $\Omega_L = 2\pi \cdot 4.3\text{MHz}$, $\Delta_L = 2\pi \cdot 1.1\text{MHz}$, $R = 2.9\mu\text{m}$). The data points are fitted with curves of damped oscillation and exponentially varied offset. Rabi oscillation occurs between two spin-down atoms and a two-qubit entangled state. There is a $\sqrt{2}$ enhancement of the microwave Rabi rate arising from the blockade, and excitation to state $|0,0\rangle$ is strongly suppressed owing to the transition blockade. The maximum Bell state $|\Psi_+\rangle$ entanglement is thus generated at around $2\mu\text{s}$.

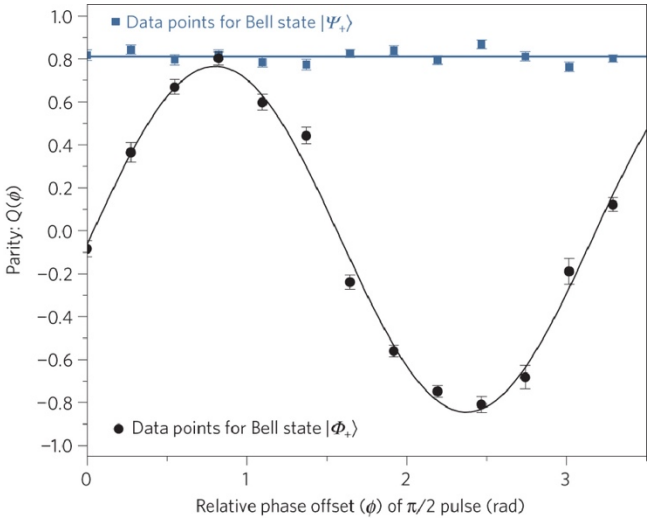

Figure 9. Entanglement verification by parity measurement [3].

Figure 9 shows the entanglement verification with the parity measurement. A global $\pi/2$ pulse is applied to the undressed system after the entangled state is prepared. $|\Psi_+\rangle$ data are fitted with a straight line, and $|\Phi_+\rangle$ data are fitted with a sinusoidal function. It shows that both Bell states generated from our experiment have a fidelity $\geq 81(2)\%$. Here, ρ represents the two-qubit density matrix. The parity measurement, $P_{1,1} + P_{0,0} - (P_{0,1} + P_{1,0})$, allows direct determination of the amplitudes of the off-diagonal elements for both entangled states. The error bars for all data points correspond to one standard deviation.

In recent work [2], the Rydberg-dressed entanglement protocol with a spin-flip blockade has been more robust by means of an adiabatic ramping technique and electric field controls. Currently, atom loss due to the admixture of the Rydberg state has been minimized because the Rydberg-dressed states can be returned to the bare ground states by adiabatically ramping the dressing laser's intensity and detuning. Furthermore, the electric field control system with electrodes enhances the Rydberg spectroscopy by means of cancelling stray electric fields and minimizing electric field drifts. We also confirm the Rydberg state lifetime ($\tau \approx 116 \pm 19\mu s$ for $54P_{3/2}[2]$) comparable to the theoretical lifetime. Finally, minimizing other experimental imperfections will improve the deterministic entanglement fidelity and open the door to more full control of complex quantum systems.

Quantum computation with a universal CPHASE gate

The possibility of quantum computation with a universal C-phase gate have been explored in the Rydberg-dressed atomic system. The Rydberg-dressed protocol suggests a new approach of entanglement between neutral atoms, and this approach is an essential part of demonstrating a universal quantum logic gate toward quantum computation.

CPHASE gate with adiabatic Rydberg-dressing protocol

We study a new scheme of implementing a controlled - Z (CZ) gate between two neutral-atom qubits, and the scheme is based on the adiabatic Rydberg-dressing protocol robust to errors caused by atomic motion. Here we summarize our work published in [4]. First, by employing adiabatic dressing of the ground electronic state, we can protect the gate from decoherence due to random phase errors that typically arise because of atomic thermal motion. Second, the adiabatic protocol allows for a Doppler-free configuration that involves counter-propagating lasers that further reduces motional errors due to Doppler shifts. Thus the residual motional error is dominated by dipole-dipole forces acting on doubly-excited Rydberg atoms when the blockade is imperfect.

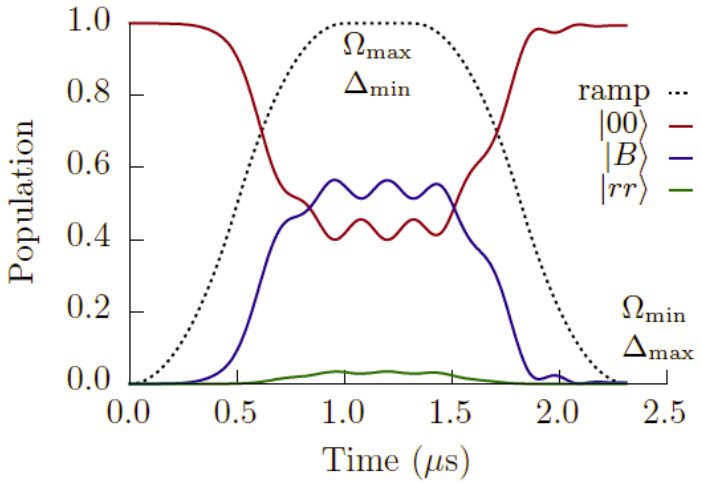

Figure 10. Adiabatic Rydberg-dressing and bare state populations [4], where $|0\rangle = |6S_{1/2}, F = 4, m_F = 0\rangle$, $|1\rangle = |6S_{1/2}, F = 3, m_F = 0\rangle$, $|r\rangle = |84P_{3/2}, m_J\rangle$, $|B\rangle = (|r0\rangle + |0r\rangle)/\sqrt{2}$ (bright state), and $|D\rangle = (|r0\rangle - |0r\rangle)/\sqrt{2}$ (dark state).

Figure 10 shows the calculation of adiabatic Rydberg-dressing (pulse shape) and bare state populations over the course of a gate with experimentally feasible parameters; pulse rise time 1μs, Rabi frequency sweep $\Omega_r/2\pi = 0 \rightarrow 3\text{MHz}$, detuning sweep $\Delta = 2\pi \cdot 6 \rightarrow 0\text{MHz}$, Rydberg decay rate $\Gamma/2\pi = 3.7\text{kHz}$ (blackbody limited lifetime), and interatomic separation $r = 5\mu\text{m}$. As the laser turns on and is tuned to resonance, the bare ground $|00\rangle$ state (red) is dressed by admixing significant bright $|B\rangle$ state (blue) population, while the blockaded $|rr\rangle$ state (green) remains mostly unpopulated. Adiabaticity and available interaction strength set comparable constraints in this case, so that the laser pulse shape that best achieves the desired evolution is neither square-topped nor triangular.

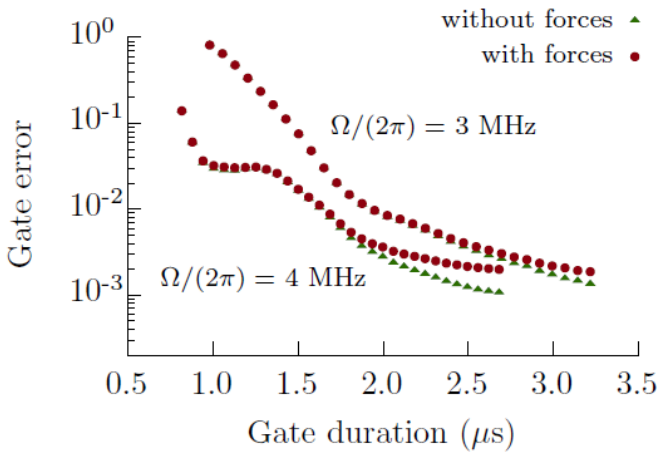

Figure 11. Simulated gate error rates $1 - \mathcal{F}$ as a function of adiabatic ramp time, considering the Rabi rate of a Rydberg excitation laser ($\Omega_r = 2\pi \cdot 3,4\text{MHz}$) [4].

Figure 11 shows the simulated gate error rates $1 - \mathcal{F}$ as a function of adiabatic ramp time is calculated for $\Omega_r = 2\pi \cdot 3\text{MHz}$ (the upper pair of curves) and $\Omega_r = 2\pi \cdot 4\text{MHz}$ (the lower pair of curves) with/without considering interatomic forces. Ignoring interatomic forces but including all other errors (green triangles), the higher Rabi rate improves both gate speed and fidelity. Including interatomic forces (red circles), any gain in fidelity from the increased speed is offset by stronger forces owing to a larger $|rr\rangle$ population when the blockade is imperfect. This suggests that beyond a certain threshold, increased laser power requires a commensurately stronger blockade interaction in order to improve fidelity.

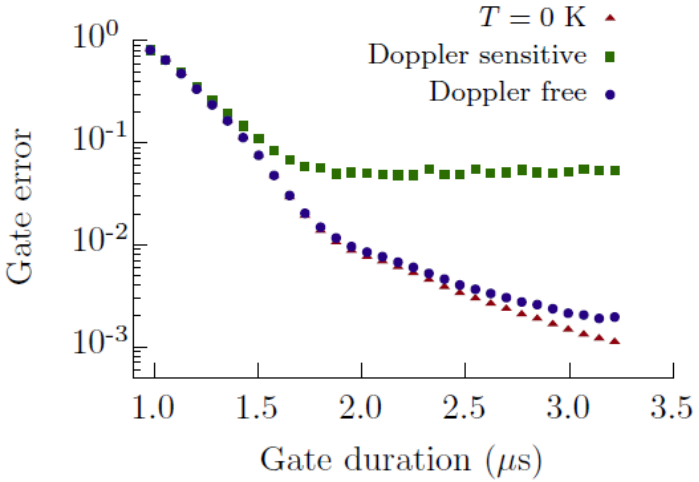

Figure 12. Simulated gate error rate as a function of an adiabatic ramp time, considering Doppler sensitive or Doppler free Rydberg excitation laser [4].

Figure 12 shows the simulated gate error rates $1 - \mathcal{F}$ as a function of adiabatic ramp time, considering motional effects and Doppler shifts. For comparison, the red triangle curve ignores motional effects and includes errors due solely to diabatic transitions and finite Rydberg lifetime. For ramp times significantly below 1μs, all curves predict low fidelities because the gate is not adiabatic. As the ramp time and adiabaticity are increased, other error sources become limiting factors. Including all error sources while using the Doppler-free configuration (blue circles), we

can reach error rate $\sim 2\times10^{-3}$, with finite blockade strength as the primary fidelity-limiting factor. By contrast, the single-laser configuration (green squares) suffers more than an order of magnitude greater error than its counterparts.

The main advantage of this approach is that it strongly suppresses random phases between bright-state $|B\rangle$ and dark-state $|D\rangle$ superpositions that arise due to atomic motion. In addition, by employing two counter-propagating Rydberg lasers, one can eliminate the Doppler shift to first order. All effects of thermal motion then take the form of coupling to a dark state outside the ideal blockade subspace, which is suppressed by an energy gap during adiabatic evolution. When both adiabatic dressing and the Doppler-free configuration are used together, errors from thermal motion are reduced by more than an order of magnitude compared to either strategy used alone.

With motional errors reduced in this way, the main remaining source of error is entanglement between internal and external degrees of freedom due to dipole-dipole forces when the Rydberg blockade is imperfect. Such error is highly nonlinear in laser power; it can be kept small as long as the Rydberg blockade is nearly perfect, but increases rapidly when laser power is increased beyond the point of breaking the blockade. This implies that the available blockade strength sets an upper limit on useful laser power, which in turn limits both the fidelity and speed of the gate. If the blockade shift can be increased by bringing atoms into closer proximity or by the appropriate choice of Rydberg levels, the gate errors will be limited solely by finite Rydberg lifetime.

As a final note, we have considered here gates performed while atoms are untrapped and fall ballistically. Recapturing the atoms after the gate will generally cause the atoms to heat. This effect is not reflected in our error estimates because it does not affect the fidelity of any one gate, but it could increase decoherence if multiple gates are performed successively with no re-cooling in between. In principle, all of these errors would be substantially reduced in a "magic trap" which traps electronic ground-state and Rydberg atoms equivalently. In that case, cooling the atoms to the vibrational ground state would completely remove Doppler shifts as well as suppress decoherence due to the dipole-dipole force in an imperfect blockade, providing a potential path to high fidelity quantum logic.

Related application of the Rydberg-dressed interaction

Rydberg-dressed ground-state atoms provide the requisite entangling interactions of quantum computation. The Rydberg-dressed interaction can be extended to a specific quantum computation application such as adiabatic quantum computation [5]. Its algorithm can be implemented by continuous transformation of the Hamiltonian from an initial form whose ground state is easy to prepare to the final form whose ground state encodes the output of the algorithm. If the energy gap between the ground and excited states is sufficiently large, the transition from initial to final Hamiltonian can be accomplished efficiently. The adiabatic quantum computation paradigm is particularly attractive because the existence of an energy gap can make the system inherently robust to certain types of errors.

Based on off-resonant Rydberg dressing of the atomic ground state instead of a resonant Rydberg π-pulse, this entangling mechanism is also more compatible with adiabatic quantum computation. The interactions are always-on and can be continuously changed to transfer from the initial to final Hamiltonian. Such adiabatic evolution has been employed in recent cold atom/ion experiments to study quantum simulations of Ising models. For an example, the implementation

of quantum annealing in an Ising spin-lattice can solve an instance of the quadratic unconstrained binary optimization (QUBO) problem.

The performance of quantum annealing to the ground state of an Ising spin-lattice has been numerically tested as a proof-of-principle experiment. Numerical simulation yield fidelities > 0.98 for up to four qubits, and implementations of $10 \sim 20$ qubits are within the range of current technology. The benchmark of the performance of a proof-of-principle realization/implementation for a few qubits operation is essential. The performance of the neutral-atom platform for adiabatic quantum computation depends on a combination of practical and fundamental questions. The minimum gap between the ground state and first excited state determines the time scale for implementing the algorithm and thus the probability of spontaneous emission, the fundamental source of decoherence. For a given problem size, the gap is constrained by J arising from the Rydberg dressing, whose optimal value for a given laser power depends on the details of the atomic level structure. For the reasonable power and detuning, we could achieve $J = 470\text{kHz}$ and a fidelity of ~ 0.99 in a proof-of-principle solution to an Ising model with ~ 4 qubits. Modest increases in this coupling would allow us to attain high-fidelity control with larger numbers of qubits. However, unlike fault-tolerant universal quantum computation in the quantum circuit model, for the purpose of solving optimization problems by quantum annealing, such high fidelity is not necessary. One requires instead the fidelity of finding the system in the ground state be sufficiently high that one can amplify the success probability with k independent trails. For our current parameters, this should allow us to explore the regime of $10 \sim 20$ of qubits, where interesting physics beyond classical simulation is accessible.

Finally, while this initial proof-of-principle analysis focused on nearest-neighbor Ising spin lattices, in principle this atomic architecture should allow us to explore more arbitrary connected graphs associated with a general QUBO problem. For example, a complete bipartite graph is isomorphic to a square crosshatch of intersecting lines, where each line represents a vertex of the graph and their intersections are the edges. This could be achieved in our system by encoding logical qubits as Rydberg-coupled one dimensional spin chains. The proximity of these spin chains to one another in a designed trapping geometry would determine the edges of the graph. Such an architecture would give substantial flexibility to explore a wide range of computationally complex Ising problems and open the door to deeper studies of quantum annealing and general adiabatic quantum computation, as we can study in future work.

Quantum control and quantum simulation

The normal-mode splitting of symmetric atomic ensembles with a Rydberg-blockade is the distinctive feature of the nonlinear coupling of the Jaynes-Cummings (JC) model. In addition, the full spectrum of the Rydberg-dressed states offers a new approach to generating more arbitrary quantum states such as arbitrary symmetric entangled states with quantum optimal control [6].

Optimal control of Rydberg-dressed atomic ensembles

We summarize here our work published in [6]. A symmetric Rydberg-dressed atomic ensemble is analogous to the JC model [2]. The role of a qubit is performed by the presence or absence of a collective Rydberg excitation from the symmetric many-body ground state atoms, and the bosonic mode manifests as the number of single atom spin flips in the ensemble. The Rydberg-dressed states are defined as the ground-like dressed state $|\tilde{g}, n\rangle$ and Rydberg-like dressed state $|\tilde{e}, n-1\rangle$ [2] as follows: $|\tilde{g}, n\rangle \equiv \cos(\theta_n/2)\,|g, n\rangle + \sin(\theta_n/2)|e, n-1\rangle$, $|\tilde{e}, n-1\rangle \equiv \cos(\theta_n/2)|e, n-1\rangle - \sin(\theta_n/2)|g, n\rangle$, where $tan\theta_n = \sqrt{n}\Omega_r/\Delta_r$; $|g, n\rangle \equiv \left\{|0\rangle^{\otimes N-n}|1\rangle^{\otimes n}\right\}_{sym}$, $|e, n\rangle \equiv \left\{|0\rangle^{\otimes N-n-1}|1\rangle^{\otimes n}|r\rangle\right\}_{sym}$. In this frame, quantum optimal control can generate arbitrary quantum states. Specifically, microwaves with a time-dependent phase are sufficient to make these ensembles completely controllable, in the sense that one can generate an arbitrary unitary transformation on the system. Here we summarize our work in [6]. We apply this to the problem of state mapping. With currently feasible parameters, it is possible to generate arbitrary symmetric states of ~ 10 hyperfine qubits with high fidelity in $\sim 1\mu s$, assuming fast microwave phase switching times. To reduce the requirements on phase switching, we propose a dressed ground control scheme, in which the control task is simplified by restricting the system's dynamics to the dressed ground subspace.

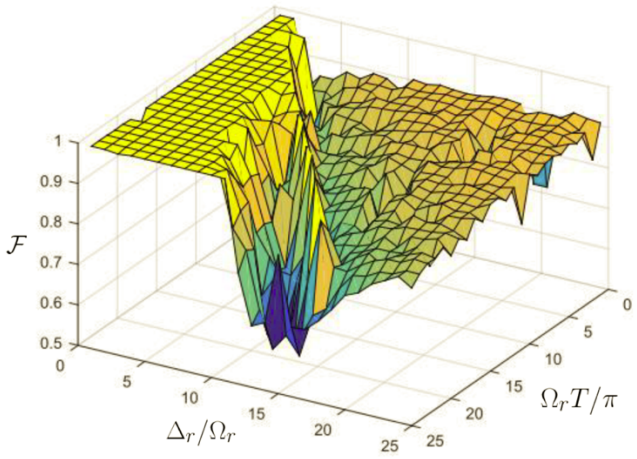

Figure 13. Simulated control fidelities to produce a 6-atom cat state in the dressed state basis [6]; $|0\rangle = \left|6S_{1/2}, F = 3, m_F = 0\right\rangle$, $|1\rangle = \left|6S_{1/2}, F = 4, m_F = 0\right\rangle$, and $|r\rangle = |nP_{3/2}, m_J\rangle$.

Figure 13 shows the simulated control fidelities to produce a six-atom cat state in the dressed basis; the state starts from $|g, 0\rangle$, as a function of Rydberg laser Δ_r and total run time T, using the minimum of $s = 25$ phase steps. For any given Δ_r, there is a "quantum speed limit,"

which determines the control time above which fidelity is arbitrarily close to one. As Δ_r increases, κ decreases and the minimum control time gets longer; $\kappa = \langle \tilde{g}, 2 | H_{JC} | \tilde{g}, 2 \rangle - 2\langle \tilde{g}, 1 | H_{JC} | \tilde{g}, 1 \rangle \approx -\Omega^4/8\Delta_r^3$ is the nonlinear shift of the ground-like dressed states related to the entangling power and the control time ($T = \pi/\kappa$). Infidelities shown here are due solely to the quantum speed limit; decoherence is not included in the simulation.

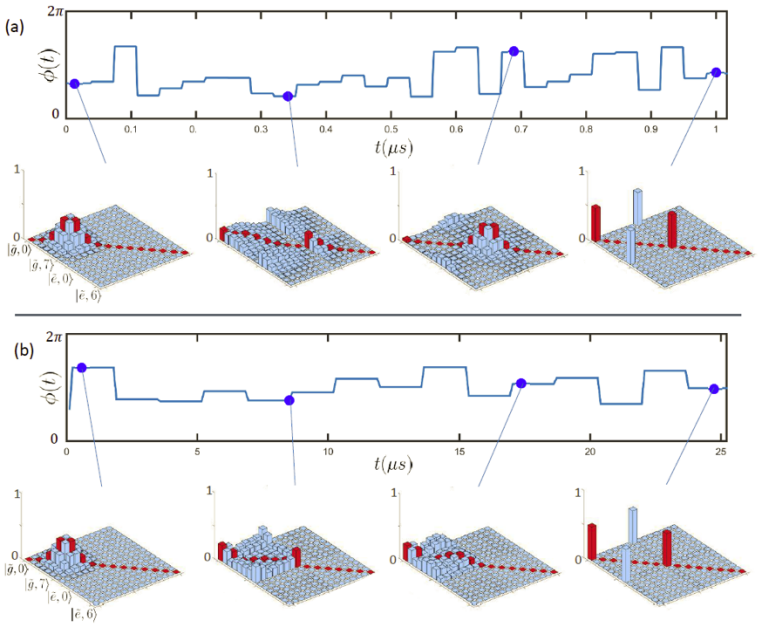

Figure 14. Mapping the 7-atom spin coherent state to the cat state in the dressed basis [6].

Figure 14 shows the quantum optimal control of a 7-atom spin coherent state $(|0\rangle + |1\rangle)^{\otimes 7}/\sqrt{2^7}$ mapped to the cat state $(|0\rangle^{\otimes 7} + |1\rangle^{\otimes 7})/\sqrt{2^7}$ in the dressed basis, with $\Omega_r/2\pi = 5\text{MHz}$. Line plots show the microwave phase $\phi(t)$ found via optimal control, and bar charts show the real part of the 15×15 density matrix at various snapshots in time. Figure 14 (a) shows full Hilbert space control, with $|\Delta_r| = \Omega_r/2$ and $\Omega_{\mu w}/2\pi = 12.5\text{MHz}$. All 15 dressed states are traversed during control, so $4N + 1 = 29$ phase steps are needed. Figure 14 (b) shows dressed ground control, with $|\Delta_r| = 3\Omega_r$ and $\Omega_{\mu w}/2\pi = 6\text{MHz}$. Population remains in the 8 dressed-ground states, so only $2N + 1 = 15$ phase steps are needed, but weaker Rydberg coupling reduces κ by more than an order of magnitude with a commensurate increase in run time.

Creating arbitrary entangled many-body quantum states is a central challenge in the field of quantum information. Beyond their intrinsic interest as highly non-classical states, such states are a crucial resource for information processing protocols, including measurement-based quantum computation, error correction, and metrology beyond the standard quantum limit. In neutral atoms, one powerful tool for generating such states is the Rydberg blockade in which the electric dipole-dipole interaction (EDDI) between high-lying Rydberg states suppresses excitation of more than one Rydberg state at a time. In this work, we apply the Rydberg blockade to the problem of many-body quantum state control. Specifically, we study the symmetric control of ensembles, in which one can produce a target entangled state by applying a Hamiltonian that acts on every atom in the ensemble equivalently. For an ensemble of N qubits, this corresponds to control on a Hilbert space spanned by the Dicke states, the symmetric subspace of N spin-1/2 particles, with total spin $J =$

$N/2$. Control and measurement of Dicke states is more tractable since the symmetric subspace grows linearly with the number of particles, whereas in a general tensor-product space, the dimension grows exponentially. This should allow us to make substantial steps in developing new tools for control and measurement of many-body systems. Dicke-state control has been demonstrated in ionic and photonic systems, and has been proposed for Bose-Einstein condensates. A simple case of two-atom symmetric control based on the Rydberg blockade was demonstrated [3] to produce Bell states.

Finally, all of the analysis in this work assumed perfectly known Hamiltonians and neglected fundamental decoherence and experimental noise. Imperfect fidelity then stems solely from imperfect control. We expect these predictions to be a good approximation as long as the control time is short compared the decoherence time, e.g. the photon scattering time, but this will put a time limit on high-fidelity control and determine the maximum ensemble size that can be realistically controlled.

Assuming decoherence can be managed for at least a few μs, controlling 10 atoms should be viable with current technology. Other experimental imperfections may be mitigated with the tools of robust control, which has been an essential tool for high fidelity control of qudits. Of particular interest are errors due to imperfect Rydberg blockade and Hamiltonian asymmetry, as they couple the ground and single Rydberg Dicke states to a larger Hilbert space. In addition, the number of atoms trapped in the ensemble can be uncertain. Tackling these challenges will require extending the tools of robust control to a Hilbert space of uncertain dimension.

Quantum simulation with a Rydberg-dressed interaction

For the pursuit of developing functional devices or understanding the properties of complex materials, simulations with exact solutions are key procedures in material science. Simulation of complex materials at the level of quantum mechanics informs many higher-level needs, providing equation-of-state information, transport coefficients, and much more. However, as the complexity of the problem continues to grow and functional materials become more prominent, so does the complexity of materials modeling efforts. Exact numerical simulation of quantum systems with classical computers generally requires resources that scale exponentially in system size. While approximate simulations may require polynomial-scaling resources, these methods do not provide error bounds. This implies that the need for quantifiably accurate simulation of quantum systems of increasing complexity will outpace the capability of classical computers, particularly in the twilight of Moore's Law. Quantum simulation is a transformative solution to this exponential bottleneck through which polynomial-scaling quantum resources can exactly simulate a quantum system in the ideal case.

Here, we consider a quantum simulator with the developed Rydberg-dressed two-atom system and the optical tweezer array. In principle, we can significantly expand the existing 2-qubit trapped-atom apparatus to be flexible enough to simulate phase transitions, non-equilibrium dynamics, and ground state energies. Our measured ZZ Rydberg-dressed interaction is real-time tunable, and thus immediately applicable to an implementation of the quantum Ising Hamiltonian, $\widehat{H} = \sum_i h_i \sigma_z^{(i)} + \sum_{j<i} J_{ij} \sigma_z^{(i)} \sigma_z^{(j)}$. As an example, we numerically calculate the solution fidelity for the ground state preparation of a 4-spin, 2D quantum Ising Hamiltonian. We find that for a square lattice with equal interactions among all pairs, $h_i = 0$, and 1% noise, a fidelity of 0.98 is

possible. A more complete space of the generalized quantum Ising model can be realized with control over the single qubit energies h_i by, for example, programming specific light shifts (local field strengths) for each atom. This can be accomplished, for example, by imaging specific patterns created by a spatial light modulator onto individual atoms.

Generalized Rydberg-dressed interaction toward quantum simulation

Moving beyond the Ising model and deeper into the quantum simulation hierarchy, the establishment of the Heisenberg model's essential components can give rise to rich entanglement phenomena that are relevant for condensed matter systems. This can be accomplished by implementing XX and YY interactions in addition to the ZZ interaction. A generalized Rydberg-dressed interaction provides a general approach to such quantum simulation.

The Rydberg-dressed interaction can be more generalized in the Bloch sphere with two Rydberg excitation fields. Two Rydberg excitation fields with any spin-spin ($\sigma_S\sigma_S$) interaction have more freedom to control the quantum states compared to single Rydberg excitation fields with a longitudinal spin-spin ($\sigma_Z\sigma_Z$) interaction. The energy-level diagrams of these Rydberg dressing schemes are displayed in Fig. 15. Two Rydberg excitation fields dressing on both qubits enable any spin-spin ($\sigma_S\sigma_S$) interaction via a stimulated Raman transition on a three level atomic system (see Fig. 15 (b)). Here $\sigma_S(\theta,\phi) = \sigma_X\cos\theta\cos\phi + \sigma_Y\sin\theta\cos\phi + \sigma_Z\sin\phi$, and we find that θ is defined by the relative optical phase between the two dressing fields, and $\phi = \arcsin\left(\frac{\Omega_1^2-\Omega_0^2}{\Omega_0^2+\Omega_1^2}\right)$. With an ideal Rydberg blockade, the spin-spin interaction Hamiltonian using the dressing scheme is then written as:

$$H_J = \frac{J}{4}\sigma_S^{(i)}\sigma_S^{(j)}, \text{ where } J = \Delta\left(\sqrt{1+\frac{\Omega_0^2+\Omega_1^2}{\Delta^2}}-1\right) - \frac{\Delta}{2}\left(\sqrt{1+\frac{2(\Omega_0^2+\Omega_1^2)}{\Delta^2}}-1\right).$$

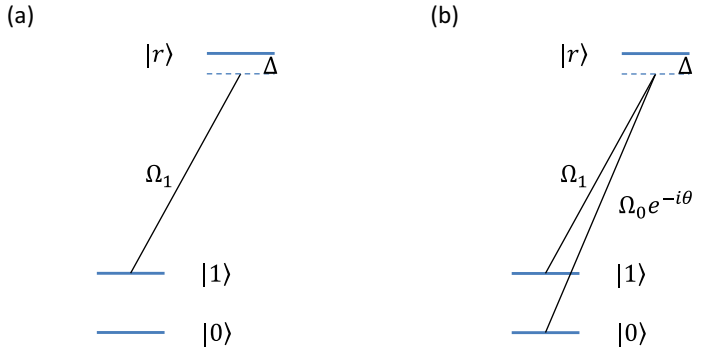

Figure 15. Energy-level diagrams of different Rydberg dressing schemes. Here, the qubit (spin) states are $|\mathbf{0}\rangle$ and $|\mathbf{1}\rangle$. The Rydberg state is $|\boldsymbol{r}\rangle$. (a) Rydberg-dressing configuration for longitudinal spin-spin ($\sigma_Z\sigma_Z$) interaction. (b) A more general Rydberg-dressing configuration for any spin-spin ($\sigma_S\sigma_S$) interaction along any direction on a Bloch sphere by using stimulated Raman transition technique.

One can see that we have a pure $\sigma_Z\sigma_Z$ interaction if either Ω_0 or Ω_1 is zero, and we can have a pure transverse spin-spin interaction if both optical Rabi frequencies for Rydberg dressing are the same ($\Omega_0 = \Omega_1$). The $\sigma_X\sigma_X$ interaction can then be obtained with $\theta = 0$. To be noted, any Rydberg dressing scheme not only introduces a spin-spin interaction, but also a single qubit (spin)

energy terms, which is not shown in the interaction Hamiltonian. In addition, the expression of J here is for ground-like dressed state. In practice, the ground-state qubits can be transformed into Rydberg-dressed qubits by ramping the frequency and the intensity of the Rydberg laser. The ground-state qubits then acquire effective interactions.

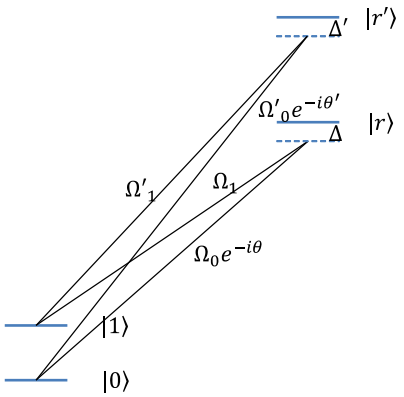

Figure 16. Energy-level diagram of the Rydberg dressing scheme with two different Rydberg states. The EDDI responses of state $|rr\rangle$, $|rr'\rangle + |r'r\rangle$, and $|r'r'\rangle$ have to be different.

In the applications of quantum computing and quantum simulation, an interaction Hamiltonian with a form of the following can be more interesting: $H_{int} = A\sigma_S^{(i)}\sigma_S^{(j)} + B\sigma'^{(i)}_S\sigma'^{(j)}_S$, where $[\sigma_S, \sigma'_S] \neq 0$, such as $H_{int} = A\sigma_X^{(i)}\sigma_X^{(j)} + B\sigma_Z^{(i)}\sigma_Z^{(j)}$. Unfortunately, it is impossible to generate this kind of interaction Hamiltonian using the scheme in Fig. 15 (b). It is, however, possible to use the dressing scheme in Fig. 16. Ideally, if the Rydberg blockade occurs only between $|rr\rangle$ and $|r'r'\rangle$ but not on $|r'r\rangle$ and $|rr'\rangle$, we can naturally produce $H_{int} = \frac{J}{4}\sigma_S^{(i)}\sigma_S^{(j)} + \frac{J'}{4}\sigma'^{(i)}_S\sigma'^{(j)}_S$, and $[\sigma_S, \sigma'_S] \neq 0$. In reality, such criterion is not guaranteed to be met, since the Rydberg energy levels of a real atom are much more complicated than an ideal few-level system. In our theoretical studies, we have established a numerical model to investigate such an idea. In order to explore different options of $|r\rangle$ and $|r'\rangle$, the computer simulation has included 10 different principal quantum numbers with S, P, and D orbitals limited by the computer resources.

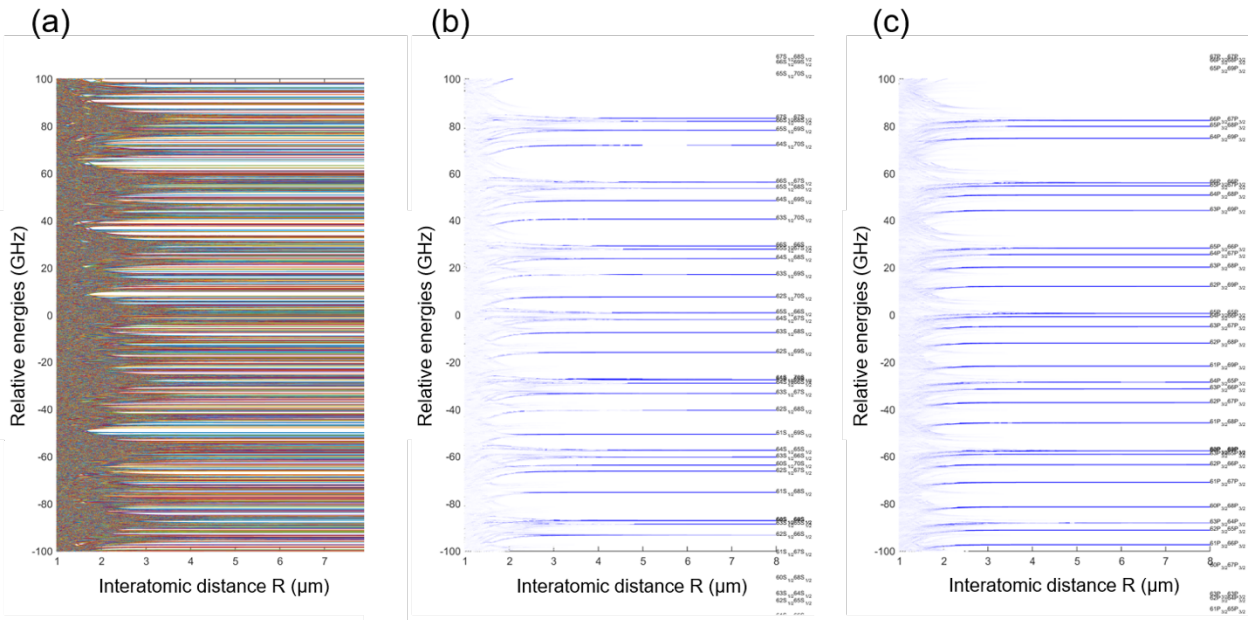

Figure 17. Rydberg energy levels. (a) Levels include all the calculated orbitals. (b) Levels of $S_{1/2}$ orbitals. (c) Levels of $P_{3/2}$ orbitals.

Figure 17 shows an example of the calculated Rydberg energy levels around the principal quantum number n near 65 for two Cs atoms as a function of interatomic distance. The illustrated two-atom Rydberg energy-level curves are plotted in Fig. 17 (a) with an energy span of 200 GHz. When $|r\rangle$ and $|r'\rangle$ are the same type of orbital but different principal quantum numbers, we can isolate those orbitals and calculate the coupling strength to the desired Rydberg levels as shown in Fig. 17 (b) and Fig. 17 (c) for $S_{1/2}$ and $P_{3/2}$ orbitals. To characterize the electric dipole-dipole interactions (EDDI) for the selected two-atom Rydberg states $|rr\rangle$, $|r'r\rangle$, $|rr'\rangle$, and $|r'r'\rangle$. We use a form of C_n/R^n to approximate the EDDI curves. By fitting the results from Fig. 17 (b) and Fig. 17 (c) with C_6/R^6 dependence, we find that for $|r\rangle = |65S_{1/2}\rangle$ and $|r'\rangle = |66S_{1/2}\rangle$, we obtain $C_6 = 200$ GHz μm^6, $C_6 = 70$ GHz μm^6, $C_6 = 220$ GHz μm^6 for $|rr\rangle$, ($|r'r\rangle$ or $|rr'\rangle$), and $|r'r'\rangle$ respectively. For $|r\rangle = |61P_{3/2}\rangle$ and $|r'\rangle = |68P_{3/2}\rangle$, we obtain $C_6 = -15$ GHz μm^6, $C_6 = -28$ GHz μm^6, $C_6 = -45$ GHz μm^6 for $|rr\rangle$, ($|r'r\rangle$ or $|rr'\rangle$), and $|r'r'\rangle$ respectively. With these EDDI potentials, we can plot J curves for different conditions as shown in Fig. 18. We then find the spin-spin interaction Hamiltonian to be: $H_{int} = \frac{1}{4}\left(J\sigma_S^{(i)}\sigma_S^{(j)} + J_c(\sigma'^{(i)}_S\sigma_S^{(j)} + \sigma_S^{(i)}\sigma'^{(j)}_S) + J'\sigma'^{(i)}_S\sigma'^{(j)}_S\right)$, where J_c is the cross interaction strength.

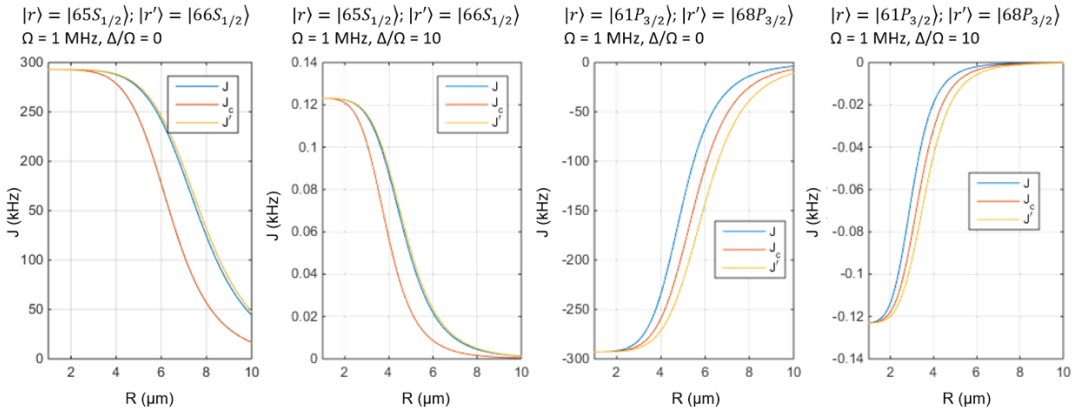

Figure 18. J curves using $|r\rangle = |65S_{1/2}\rangle$ and $|r'\rangle = |66S_{1/2}\rangle$; and $|r\rangle = |61P_{3/2}\rangle$ and $|r'\rangle = |68P_{3/2}\rangle$.

In Fig. 18, the effective Rabi frequency is defined as $\Omega^2 = \Omega_0^2 + \Omega_1^2 = \Omega'^2_0 + \Omega'^2_1$. As we can see from Fig. 18, it does not lead to zero EDDI for $|r'r\rangle$ and $|rr'\rangle$ and thus vanishing J_c. However, using different Rydberg states for $|r\rangle$ and $|r'\rangle$ does provide a different type of spin-spin H_{int}. This may still benefit quantum simulations for some specific problems. The calculation examples shown here only illustrate $|r\rangle$ and $|r'\rangle$ with the same orbital angular momentum. For $|r\rangle$ and $|r'\rangle$ with different orbitals, for example S and P, S and D, P and D, etc., have also been investigated. However, we have not found a good combination, which leads to a very small J_c for the optimal interatomic distance with Cs atoms.

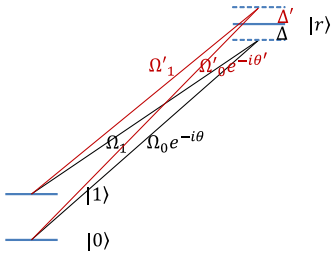

Figure 19. A Rydberg-dressing scheme to produce $\sigma_X^{(i)}\sigma_X^{(j)} - \sigma_Y^{(i)}\sigma_Y^{(j)}$, $\sigma_Y^{(i)}\sigma_Y^{(j)} - \sigma_Z^{(i)}\sigma_Z^{(j)}$, or $\sigma_Z^{(i)}\sigma_Z^{(j)} - \sigma_X^{(i)}\sigma_X^{(j)}$.

Now we are going to consider another dressing scheme that can give us a specific H_{int} with two spin-spin interaction terms but no cross terms. In Fig. 19, we use a single Rydberg state for dressing but two pairs of dressing fields with opposite optical detunings. Assuming there are two independent Rydberg-dressed interactions produced with $J = -J'$, we then find the interaction Hamiltonian to be $H_{int} = \frac{J}{4}\left(\sigma_S^{(i)}\sigma_S^{(j)} - \sigma'^{(i)}_S\sigma'^{(j)}_S\right)$. More dressing schemes for specific spin-spin or qubit-qubit interactions can possibly be found. But this will require a more careful analysis of the collective two-atom light-shift effects depending on the optical polarization, Rydberg sublevels, etc.

One basic requirement for enabling $\sigma_X\sigma_X$ or any spin-spin interaction with transverse components is to have two-color Rydberg dressing to match the energy splitting between the two qubit states. For direct UV Rydberg excitation to P orbitals, this can be very challenging especially when the qubit is encoded in a pair of ground-state hyperfine sublevel with a splitting energy in the microwave frequency domain, because optical modulation components at UV wavelengths are

not convenient to find. Without direct modulation to the UV laser, multiple UV laser systems need to be set up, and phase locking between lasers will be required. This leads to a higher equipment cost for the experiment. In addition to the challenges of multi-frequency laser technology, it is very important to maintain a good stability of Rydberg-dressing lasers especially when it is involved with the transverse spin-spin interactions. Any relative noise between the qubit transition frequency and the driving frequency from the stimulated Raman transition can cause effective dephasing. Nevertheless, we believe that those technical challenges are resolvable. The Rydberg-dressed interaction then will be no longer limited to a $\sigma_Z\sigma_Z$ type interaction and many other possible combinations will be possible.

The Rydberg-dressed interaction between cold neutral atoms provides a natural protocol for quantum simulation of condensed-matter physics. In addition, the generalized Rydberg-dressed interaction with two Rydberg excitation fields enables tunable, anisotropic interactions, which can open the door to quantum simulations of a variety of exotic quantum phases.

LISTS OF PUBLICATIONS, TECHNICAL ADVANCES AND PROVISIONAL PATENTS

Publications

1. Jongmin Lee, Michael J. Martin, Yuan-Yu Jau, Tyler Keating, Ivan H. Deutsch, and Grant W. Biedermann, Demonstration of the Jaynes-Cummings ladder with Rydberg-dressed atoms, under review, arXiv:1609.03940 (2016)
2. Tyler Keating, Charles H. Baldwin, Yuan-Yu Jau, Jongmin Lee, Grant W. Biedermann, Ivan H. Deutsch., Arbitrary Dicke-State Control of Symmetric Rydberg Ensembles, accepted Phys. Rev. Lett., arXiv:1607.03169 (2016).
3. Y.-Y. Jau, A. M. Hankin, T. Keating, I. H. Deutsch, G. W. Biedermann, Entangling Atomic Spins with a Strong Rydberg-Dressed Interaction, Nature Physics, 12, 71 (2016).
4. Tyler Keating, Robert L. Cook, Aaron Hankin, Yuan-Yu Jau, Grant W. Biedermann, Ivan H. Deutsch, Robust quantum logic in neutral atoms via adiabatic Rydberg dressing, Phys. Rev. A 91, 012337 (2014). *Editor's Suggestion*

Presentations

Listed below are the invited and contributed presentations associated with this work.

Invited

1. American Physical Society, 4 corners meeting, Las Cruces, NM, 2016
2. Frontiers of Matter Wave Optics, Arcachon, France, 2016
3. American Physical Society, Division of Atomic, Molecular and Optical Physics (DAMOP) meeting, Rhode Island, 2016
4. AMO seminar, Rice University, Houston TX, 2016
5. International conference on Rydbergs in Durham (iCorD), Durham U.K., 2015
6. Group seminar, M. Kasevich group, Stanford University, 2015
7. Group seminar, Air Force Research Labs, Albuquerque NM, 2015
8. Science and engineering in quantum information systems (SEQIS) research challenge, Sandia National Laboratories, 2014
9. Center for quantum information and control (CQuIC) seminar, University of New Mexico, 2014

Contributed

1. American Physical Society, Division of Atomic, Molecular and Optical Physics (DAMOP) meeting, 2014
2. Squint (Southwest Quantum Information and Technology conference), 2015
3. American Physical Society, Division of Atomic, Molecular and Optical Physics (DAMOP) meeting, 2015
4. Squint (Southwest Quantum Information and Technology conference), 2016

Technical Advance

1. “Method and apparatus for quantum information processing using entangled neutral-atom qubits”, disclosed 10/27/2010, Sandia Disclosures SD13355.0/S139511

Provisional Patent

1. US Appln. No.: 62/265,579; Method and apparatus for quantum information processing using entangled neutral-atom qubits

CONCLUSIONS

We have developed a new approach to entangling neutral atoms with a Rydberg-dressed interaction that can be extensively applied in quantum technology goals such as quantum computation, many-body quantum simulation, and high-precision atomic sensors. The demonstrated Rydberg-dressed interaction enables a strong and tunable dipole-dipole interaction between individually trapped atoms with energy shifts of order 1 MHz which is challenging to achieve in other protocols. Using this interaction, we experimentally demonstrated Bell state entanglement and a spectroscopic mapping of the Jaynes-Cumming model for symmetric Rydberg ensembles. Furthermore, we developed theoretical studies of a Rydberg-dressed atomic system for a universal CPHASE quantum logic gate, and arbitrary Dicke state quantum control of symmetric atomic ensembles. With continued refinement, we expect that Rydberg-dressed states will offer a favorable approach to creating large scale entanglement, quantum simulation, operating high-fidelity phase gates, and generating arbitrary quantum states using optimal control. With the advent of highly efficient single-atom loading [7] and array-assembly techniques [8], one can clearly envision symmetric interactions for an ensemble of ~100 atoms in 2D/3D lattices [8-11] when constrained by a modest ~ 10 um Blockade radius [12, 13]. In the context of quantum computing as well as asymmetric interactions, system sizes can reach far beyond [14].

REFERENCES

1. A. M. Hankin, Y.-Y. Jau, L. P. Parazzoli, C. W. Chou, D. J. Armstrong, A. J. Landahl, and G. W. Biedermann, "Two-atom Rydberg blockade using direct 6S to nP excitation," Phys. Rev. A, **89**, 033416, (2014).
2. Jongmin Lee, Michael J. Martin, Yuan-Yu Jau, Tyler Keating, Ivan H. Deutsch, Grant W. Biedermann, "Demonstration of the Jaynes-Cummings ladder with Rydberg-dressed atoms," under review, arXiv:1609.03940 (2016).
3. Y.-Y. Jau, A. M. Hankin, T. Keating, I. H. Deutsch, and G. W. Biedermann, "Entangling atomic spins with a Rydberg-dressed spin-flip blockade," Nature Physics, **12**, 71-74 (2016).
4. Tyler Keating, Robert L. Cook, Aaron M. Hankin, Yuan-Yu Jau, Grant W. Biedermann, and Ivan H. Deutsch, "Robust quantum logic in neutral atoms via adiabatic Rydberg dressing," Phys. Rev. A, **91**, 012337 (2015).
5. Tyler Keating, Krittika Goyal, Yuan-Yu Jau, Grant W. Biedermann, Andrew J. Landahl, and Ivan H. Deutsch, "Adiabatic quantum computation with Rydberg-dressed atoms," Phys. Rev. A **87**, 052314 (2013).
6. Tyler Keating, Charles H. Baldwin, Yuan-Yu Jau, Jongmin Lee, Grant W. Biedermann, Ivan H. Deutsch, "Arbitrary Dicke-State Control of Symmetric Rydberg Ensembles," accepted Phys. Rev. Lett., arXiv:1607.03169 (2016).
7. Brian J. Lester, Niclas Luick, Adam M. Kaufman, Collin M. Reynolds, and Cindy A. Regal, Phys. Rev. Lett. **115**, 073003 (2015).
8. D. Barredo, S. de Léséleuc, V. Lienhard, T. Lahaye, and A. Browaeys, arXiv:1607.03042 (2016).
9. J. Zeiher, P. Schauß, S. Hild, T. Macr`ı, I. Bloch, and C. Gross, Phys. Rev. X 5, 031015 (2015).
10. Y. Wang, X. Zhang, T. A. Corcovilos, A. Kumar, and D. S. Weiss, Phys. Rev. Lett. 115, 043003 (2015).
11. Y. Wang, A. Kumar, T.-Y. Wu, and D.S. Weiss, Science 352, 1562 (2016).
12. M. J. Piotrowicz, M. Lichtman, K. Maller, G. Li, S. Zhang, L. Isenhower, and M. Saffman, Phys. Rev. A 88, 013420 (2013).
13. F. Nogrette, H. Labuhn, S. Ravets, D. Barredo, L. Be-guin, A. Vernier, T. Lahaye, and A. Browaeys, Phys. Rev. X 4, 021034 (2014).
14. M. Saffman, J. Phys. B: At. Mol. Opt. Phys. 49, 202001 (2016).

DISTRIBUTION

1	MS0899	Technical Library	9536 (electronic copy)

For LDRD reports, add:

1	MS0359	D. Chavez, LDRD Office	1911

For CRADA reports add:

1	MS0115	OFA/NFE Agreements	10012

For Patent Caution reports, add:

1	MS0161	Legal Technology Transfer Center	11500


Sandia National Laboratories